EXPLORATION OF THE DOUBLE PENDULUM

Jacob BLUMOFF

Georgia Institute of Technology, Atlanta, Georgia

Abstract

The double pendulum is a classic system in the study of chaos. We have explored the double pendulum experimentally, and compared results to a numerical simulation. This comparison was done in the time it takes for the second arm of the pendulum to "flip," based on initial starting conditions. We also performed analyis of the vertically driven case.

Contents

1. Introduction
2. Theory
3. Experiment
4. Data Analysis
5. Numerical Modeling
6. Results & Discussion
7. References

1. Introduction

The double pendulum is a classic example of a chaotic system (refs [1,2]). It consists of two swinging pendula, one free to swing from a fixed point, and one free to swing from the end of the first pendulum. Motion is determined by the influence of gravity on the systems four dimensional phase space: The two angles and their respective angular velocities. While we examine the standard double pendulum, we also examined the vertically driven double pendulum. In this system the mounting point of the first arm is not fixed, but oscillates vertically due to an external force. The phase space becomes quite complex. Fig. 1 describes the system (from ref. [3]), and we will now define the pertinant variables. We define l as the distance from the center of mass of the first arm to the axis of rotation of the second arm. b_1 and b_2 represent the distances from each arm's mounting point to its respective center of mass. ϕ_1 and ϕ_2 represent the angles the pendula from the vertical, and ω_1 and ω_2 are their angular velocities. m_1 and m_2 are their respective masses, and ρ_1 and ρ_2 are their uniform mass densities. The vertical displacement is sinusoidal, described as

$$\text{vertical displacement} = a\sin(\Omega t) \tag{1}$$

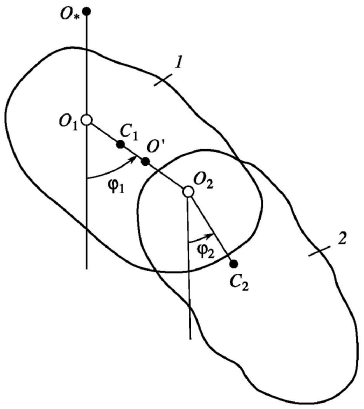

Fig. 1.

2. Theory

The theory has been described in detail in refs 3 and 4. Using the variables defined above, the kinetic and potential energies are given here.

$$\begin{aligned} T = &\frac{1}{2}(m_1\rho_1^2 + m_2l^2)\dot{\phi_1}^2 + \frac{1}{2}m_2\rho_2^2\dot{\phi_2}^2 + m_2lb_2\dot{\phi_1}\dot{\phi_2}\cos(\phi_1 - \phi_2) \\ &- ((m_1b_1 + m_2l)g\dot{\phi_1}\sin(\phi_1) + m_2b_2\dot{\phi_2}\sin(\phi_2))a\Omega\cos(\Omega t) \end{aligned} \tag{2}$$

$$H = -(m_1b_1 + m_2l)g\cos(\phi_1) - m_2b_2g\cos(\phi_2) \tag{3}$$

Momenta are introduced.

$$p_{\phi 1} = \frac{\partial T}{\partial \dot{\phi_1}} \qquad p_{\phi 2} = \frac{\partial T}{\partial \dot{\phi_2}} \tag{4}$$

$$\hat{p}_{\phi 1} = p_{\phi 1} + (m_1b_1 + m_2l)a\Omega\cos(\Omega t)\sin(\phi_1) \tag{5}$$

$$\hat{p}_{\phi 2} = p_{\phi 2} + m_1 2b_2a\Omega\cos(\Omega t)\sin(\phi_2) \tag{6}$$

From Lagranges equations, the equations of motion are produced.

$$\dot{\phi_1} = \frac{\rho_2^2\hat{p}_{\phi 1} - lb_2\cos(\phi_1 - \phi_2)\hat{p}_{\phi 2}}{m_1\rho_1^2\rho_2^2 + m_2l^2(\rho_2^2 - b_2^2\cos^2(\phi_1 - \phi_2))} \tag{7}$$

$$\dot{\phi_2} = \frac{(m_1\rho_1^2 + m_2l^2)\hat{p}_{\phi 2} - m_2lb_2\cos(\phi_1 - \phi_2)\hat{p}_{\phi 1}}{m_2(m_2\rho_1^2\rho_2^2 + m_1l^2(\rho_2^2 - b_2^2\cos^2(\rho_1 - \rho_2)))} \tag{8}$$

In the modeling section, these equations are integrated to make predictions.

In ref. [3] Kholostova shows that there are four fixed points, corresponding to the four possible vertical alignments of the two arms. Both arms at 0 degrees is stable, both arms at 180 degrees is unstable, as is intuitive. Surpisingly, the two "folded" cases, with

one arm at 0 degrees and the other at 180 degrees are found to be stable given a sufficient driving frequency.

$$\Omega^2 > \frac{2gl_1}{a^2} \tag{9}$$

This is physically similar to the stability of the vertically driven inverted pendulum, discussed in ref. [5]. Kholostova goes on to mathematica rule out the existance of any other fixed points or stable orbits (ref. [3]).

3. Experiment

The apparatus is built on a frame mounted atop an electromagnet, essentially a speaker. To drive the system vertically, a function generator is fed into an amplifier which provides the current for the electromagnet, causing the frame to oscillate. The first arm is suspended from the frame, free to turn 360 degrees. The first arm consists of two bars of aluminum, approximately 0.3 meters long and 0.2 Kg in mass. At the far end of the first arm the second arm is mounted, also free to turn 360 degrees. This arm is one aluminum bar, approximately 0.3 meters long and 0.1 Kg in mass. At the end of the bar is a 1 Kg lead weight, optionally attached. The device was constructed to be as low friction as possible. The driving mechanism can operate up to approximately 6 Hz, and at an amplitude of up to approximately 0.05 meters.

3.1. Accelerometry

Data collection was attempted in a number of ways. First, an accelerometer (Analog Devices ADXL321, rated to $\pm 18g$) attached to the lower arm was used. It yielded the acceleration of the lower arm along its radial and angular directions, logged at up to 600 Hz. This method had several flaws. First, the rotating and moving reference frame made it difficult to analyse in the lab frame. Secondly, the data had low resolution and were extremely noisy. Though high frequency filters helped, the data were still far from ideal.

3.2. High-Speed Camera

The second method of data collection attempted was to use a high frequency camera (100Hz). We then tracked an LED on the lower arm through home-built National Instruments LabView software. This method was useful in some limited situations, but the LED would move behind part of the frame or the first arm and become difficult to track. Also, the mere position of the LED is not enough information to determine the angles of both arms with certainty.

The third method was to track a high-contrast stripe of tape on the lower arm. The slope of this line, along with the length of the upper arm and the location of the mounted axis of the upper arm, determines both angles. As the line was tens of centimeters longon the order of ten centimeters long, its slope could generally be found even when the stripe was partially obscured. This collection method was by far the most effective for our purpose. An unfortunate side effect of this method was that we could no longer process data in real-time.

4. Data Analysis

The output of the highspeed camera is a series of 320x240 pixel 8-bit greyscale images at 100 frames/sec. A substantial amount of postprocessing is required to retrieve meaningful data from these files. Fist we discuss the tracking of the undriven case, then move on to the adjustments necessary for the driven case. The postprocessing was done in MATLAB and its extensions. The aperture on the camera was adjusted such that the image what highly washed out, and the line taped to the second arm is more or less the only non-white pixels.

4.1. Undriven Case

The image is converted into a completely binary image by using a threshold. The "thin" morph is applied, followed by the "skeleton" morph, resulting in a thin, continuous line tracking the original tape from the video. The "endpoint" morph is used to isolate pixels that are touching only one other non-white pixel. From there a linear regression through the endpoints finds the angle of the lower arm, and a centroid is found which gives the location. The equations to decide a flip as as follows.

$$\begin{aligned} sgn(m_{i-1}) &\neq sgn(m_{i-1}) \\ |m|_{i-1} &> 1 \\ |m|_i &> 1 \\ (x_{sus} - x_{cent})^2 + (y_{sus} - y_{cent})^2 &< \ell_1^2 \end{aligned} \tag{10}$$

In equation 10, x_{sus} and y_{sus} refer to the x and y coordinates of the suspension point of the upper arm, while x_{cent} and y_{cent} refer to the x and y coordinates of the centroid of the second arm. This gives the frame of the flip, however to determine the time to flip the frame of release is also needed. Unfortunately, we have not been able to do that in software, and it was done manually. Determining the angle of the lower arm is all that is necessary to determine a flip of the lower arm, however we also found the data for the angle of the upper arm. The procedure for doing so is as follows.

1. Find the points of intersection between the line through the endpoints of the lower arm and the circle traced by the far end of the upper arm, $(x_{sus}-x)^2+(y_{sus}-y)^2 = \ell_1^2$. One of these points is the location of the joint between the first and second arms of the pendulum.
2. If $(x_{sus} - x_{cent})^2 + (y_{sus} - y_{cent})^2 > \ell_1^2$, the point identified which is closer to the centroid is the joint, whose coordinates are x_{joint} and y_{joint}.

Given the location of the joint between the upper and lower arm and the location of the suspension axis of the upper arm, the location and angle of the upper arm are also fully determined. It should be noted that the state is not fully determined, as we have no data on the angulare velocities.

4.2. Driven Case

In the driven case there is the new challenge of tracking the suspension point of the first arm. If this point can be properly tracked, the locations and angles of the two arms can both be determined by slight modifications of the above techniques, as can the phase and amplitude of the driving force. The key issue faced here is that the vertical displacement is a small value compared to our resolution.

5. Numerical Modeling

The focus of the numerical modeling section is measuring the time it takes the second arm to flip based on different initial conditions. Instead of scanning a four dimensional parameter space, we set both intial angular velocities to zero and focus only on initial angle. The flip is defined as the absolute value of ϕ_2 reaching 180 degrees, where zero degrees is the second arm hanging straight down. Of course, a flip requires a certain degree of potential energy to reach. Atssuming the ground state energy to be zero, the minimum energy to reach a flipping configuration is given by

$$E_{Minimumtoflip} = [(m_1 b_1) + m_2(l - b_2)]g \tag{11}$$

Since the initial angular velocities are zero, the starting energy of the system is the sum of the gravitational potential energies of the two arms, given by equation (3). If the initial gravitational energy is less than the minimum energy to flip, the simulation of those initial states need not be run. While this eliminates many starting cases, it does not guarantee that all remaining cases will definitively flip in finite time. It is not necessary to scan both ϕ_1 and ϕ_2 initial conditions through -180 to 180 degrees, as the physics are symmetric for ϕ_1.

5.1. WorkingModel2D

The time to flip can clearly not be found analytically, so numerical integration is called for. Two integration schemes were used. The first applied was the creation of a model in WorkingModel2D. The physical situation was built in WorkingModel2D's built in, BASIC-based programming language, WMBasic. In BASIC loops were scanned through ranges of initial conditions, waiting until the system flipped or a certain time limit was reached. This method had several flaws. Most notably, as far as we could discover there was no way to make the integration run faster than real-time. With this model we scanned both $\phi_{1,init}$ and $\phi_{2,init}$ through 0 to 180 degrees in 1 degree steps. Also, pruning was applied, not by gravitational potential energy, but through a more crude method. This scan took approximately 12 hours of computer time. While the integrator for WorkingModel2D is as accurate as requested of it, WMBasic will only allow access to the data in larger steps than would be desirable, leading to a lack of resolution. The data are plotted in Fig. 5.1, where the axes represent different starting angles and the shade of the pixel represents time to flip. A closer region was scanned in 5.1 with a 0.1 degree step, showing the fractal nature of these data.

5.2. MATLAB

The second integration scheme was simply integrating the equations of motion given in equations (7) and (8). Since this is in the undriven case, a is set to zero. While some preperatory work was done in Mathematica, the integration itself was done in MATLAB using fourth order Runge-Kutta algorithm with a 0.001 second timestep. MATLAB allowed much finer control than WMBasic. We scanned ϕ_1 from 0 to 180 degrees, and ϕ_2 from 0 to 180 degrees, in approximately 1 degree steps. The results are plotted.

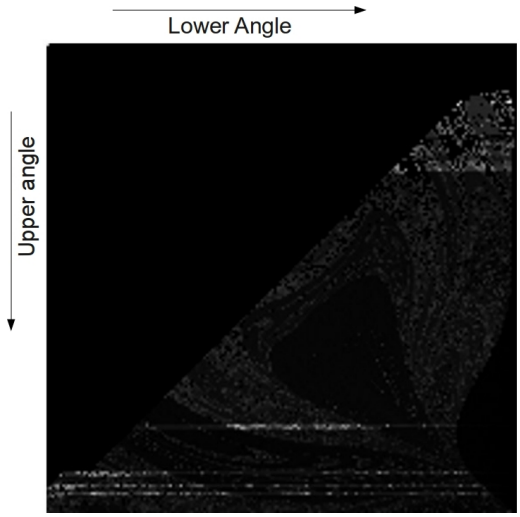

Figure 1: Working Model data depicting time to flip based on initial conditions, axes are starting angles from 0 to 180 degrees. Shade represents time to flip, lighter is faster.

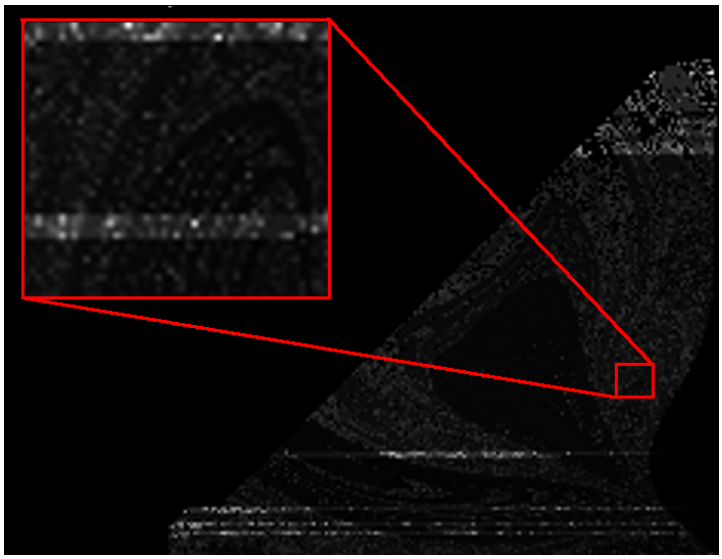

Figure 2: A higher resolution segment of the working model data shows the fractal nature of these data.

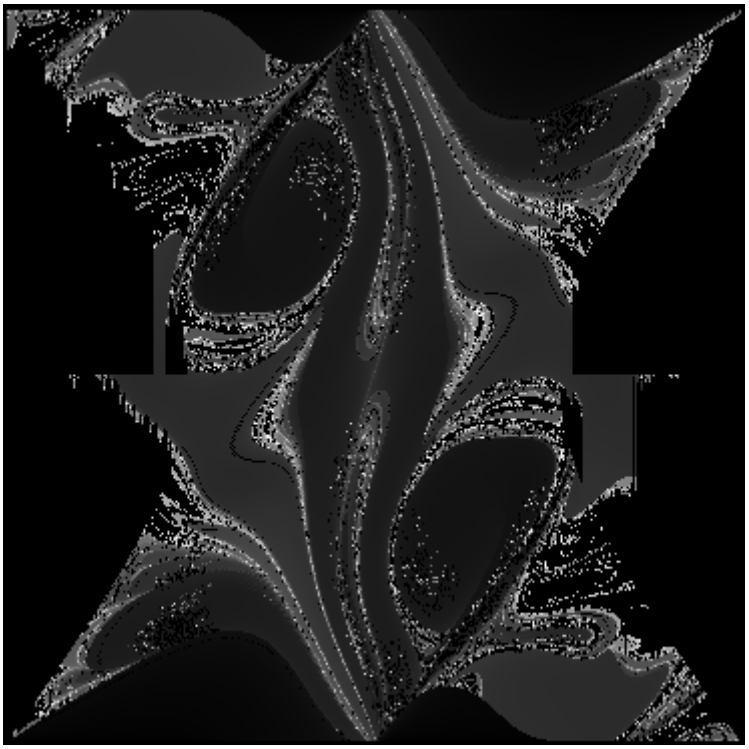

Figure 3: The MATLAB model generated this result, the first arm initial condition (horizontal axis) from - to -180 then from 180 to 0 degrees, and the second arm (vertical axis) from -180 to 180 degrees in approximately 1 degree steps. Lighter points flipped faster.

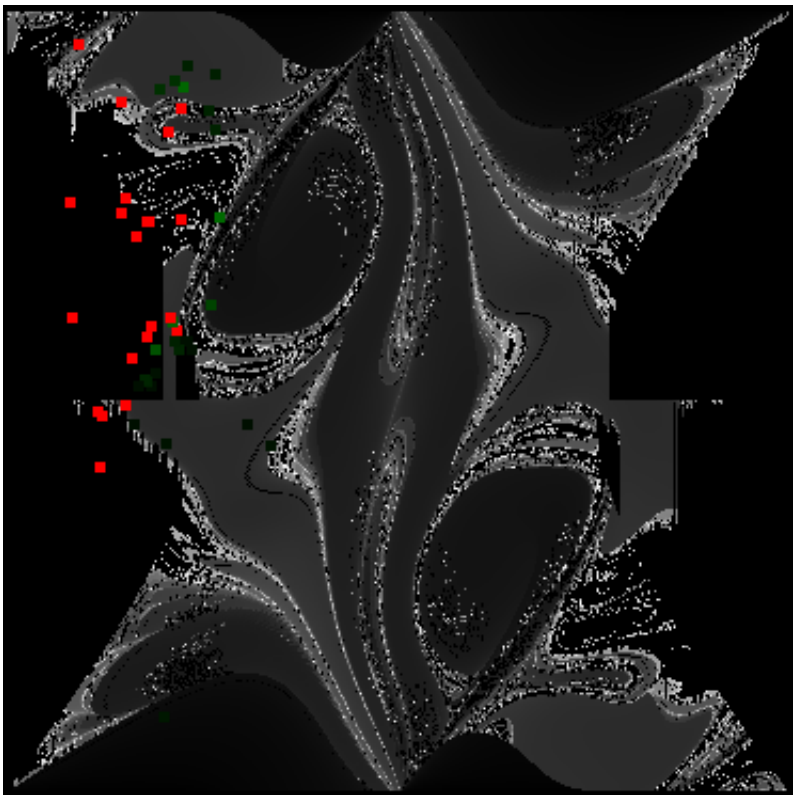

Figure 4: This shows the experimental data overlayed on the modeling data, where red corresponds to not flipping, and green indicates time to flip by intensity.

6. Results & Discussion

Our primary result is experimentally how long it took to flip based on intial conditions. That data is provided as an overlay on the computer-generated model. This matches many of the same general features as the model. Unfortunately we have far too few datapoints, and even the data we do have lacks the precision what we could generate numerically. Generally, however, we do see that the same areas flip or do not flip. With friction and damping losses in the physical experiment, edge and slow cases will switch from flipping to not flipping.

There may indeed be usefulness in studying the double pendulum beyond simply an academic exercise. Dynamic stability, first discussed in ref. [7], could be an effective tool in engineering applications. Studying how situations can be made more stable by driving them, rather than damping them could be quite useful. Unfortunately our apparatus could not reach the necessary driving conditions to examine this driven stability. Exploring these bifurcations is the next step in studying the driven double pendulum. It would be good to study the timescale of return from perturbation and range of stability based on different driving frequencies, amplitudes, and mass distributions.

7. References

[1] Troy Shinbrot, Celso Grebogi, Jack Wisdom, and James A. Yorke, "Chaos in a double pendulum," Am. J. Phys., vol. 60, no. 6, pp. 491-499, June 1992.

[2] S. Strogatz, Nonlinear Dynamics and Chaos, Westview, 1994.

[3] O. V. Kholostova, "On the motions of a double pendulum with vibrating suspension point," Mechanics of Solids, vol. 44, no. 2, pp. 184-197, April 2009.

[4] P. Qu, Q. Bi, ANALYSIS OF NON-LINEAR DYNAMICS AND BIFURCATIONS OF A DOUBLE PENDULUM, J. of Sound and Vibration, 217(4), 697-736, 1998

[5] L.D. Landau and E.M. Lifshitz, Course on Theoretical Physics, Vol. 1: Mechanics (Nauka, Moscow, 1965: Pergamon Press, Oxford, 1976).

[6] R. B. Levien and S. M. Tan, "Double pendulum: An experiment in chaos," Am. J. Phys., vol. 61, no. 11, pp. 1038-1044, November 1993.

[7] A. Stephenson, "On a New Type of Dynamical Stability," Mem. Proc. Manch. Lit. Phil. Soc. 52, Pt. 2 (8) 1-10(1908).